Narrow-Line and Broadband Spectra of Iridium(III) Complexes in a Shpol'skii Matrix and an Amorphous Host

Alfred P. Marchetti,[†] Joseph C. Deaton,*[,‡] and Ralph H. Young[†,§]

Research & Development, Eastman Kodak Company, Rochester, New York 14650, and Department of Chemistry, University of Rochester, Rochester, New York 14627

Received: October 28, 2005; In Final Form: May 4, 2006

Narrow-line emission and excitation spectra of the lowest triplet state have been studied in a Shpol'skii host (*n*-octane) for three cyclometalated IrL_2acac complexes of current practical interest. The ligands L and acac are the C-deprotonated anions of 2-phenylpyridine, 2-benzothienylpyridine, 1-phenylisoquinoline, and acetylacetone. The occurrence of narrow lines is surprising for such nonplanar structures. Individual triplet sublevels are identified, and a striking intensity effect is observed in a magnetic field. Broadband spectra and lifetime data of the complexes in PMMA yield additional properties of the individual sublevels—radiative and nonradiative decay rates and emission spectra. The data are consistent with the assumption that these individual rates and spectra are approximately independent of temperature. For each complex, the decay rates vary by a factor of ≥ 20 among the three sublevels, and that of the lowest sublevel is the smallest, but rates of radiative and nonradiative decay generally vary in parallel for all three sublevels. The individual sublevels have significantly different spectra. These regularities appear to be universal characteristics of Ir(III) and Pt(II) complexes. They cannot be explained solely on the basis of the symmetries of the electronic states because the symmetry of the present complexes is too low.

1. Introduction

Cyclometalated complexes of Ir(III), and to a lesser degree, Pt(II), are under intensive development as luminescent dopants in organic light-emitting diodes (OLEDs).[1−3] They typically exhibit highly efficient phosphorescence, making it possible to extract light from all recombination events, regardless of the spin state of the recombining electron−hole pair. In fact, internal quantum efficiencies approaching 100% have been reported for such Ir(III) complexes.[4,5] Although the excited-state lifetimes of these phosphorescent materials are long, compared to those of typical fluorescent OLED dopants, they are still short enough (ca. 1 μs) for these dopants to be of practical use, and the phosphorescence quantum yields are often high (≥ 0.5).[6−14] The properties of the electronic structure that are responsible for these attributes are of great practical interest. The photophysics of the lowest triplet level have been investigated at the level of structure−activity relationships[9,10,15−23] for numerous Ir(III) and Pt(II) complexes; and finer details, such as properties of the three individual sublevels, have been investigated for several complexes.[24−33] The controlling features are thought to be the 5d transition metal and the occurrence of a singlet metal-to-ligand charge-transfer (MLCT) state, close in energy, to the emitting triplet state. Quantum-chemical computations find that the lowest excited states are singlets and triplets with variable degrees of MLCT and ligand-centered character. Although the states are delocalized over the entire molecule, within narrow energy ranges there are at least as many states of each multiplicity as there are cyclometalating ligands.[34−36]

The facial (*fac*) isomers of complexes of Ir(III) with three ligands (L) connected to the central iridium atom via strong Ir−C and Ir−N σ bonds, i.e., *fac*-IrL_3, are of greatest interest as OLED dopants. The archetype is the complex of Ir(III) with 2-phenylpyridine (L = ppy), namely *fac*-$Ir(ppy)_3$. The emission from this complex is green, but other choices of ligand result in emission colors ranging from blue to red. Compounds in which one such ligand is replaced by an acetylacetonate (acac), i.e., IrL_2acac, have photophysical properties very similar to those of the corresponding *fac*-IrL_3, and they have served as model compounds. The present study focuses on three such compounds, $Ir(ppy)_2$acac, $Ir(btp)_2$acac, and $Ir(piq)_2$acac, where btp and piq are the C-deprotonated anions of 2-pyridylbenzothiophene and 1-phenylisoquinoline. The structures of these compounds are shown in Chart 1.

Detailed spectroscopic examination of molecular triplet states is usually done at cryogenic temperatures, and the material of interest is usually present either as a single crystal or as a dilute substitutional impurity in an inert single-crystal host (see, for instance, refs 26 and 37−40). An alternative that avoids the need to grow high-quality crystals, the Shpol'skii method, employs a polycrystalline host, usually a linear alkane and, most often, *n*-octane.[41,42] This matrix eliminates much of the inhomogeneous broadening that normally occurs in amorphous hosts or in glass-forming solvents at low temperature.[43,44] In favorable cases, molecules of the host pack around the molecules of interest in a few specific ways, resulting in a small number of discrete molecular environments ("sites"). Moreover, the guest−host interactions tend to be small, with the result that each site exhibits narrow-line emission, absorption, and excitation spectra with high information content. This situation is found most often with planar molecules such as polycyclic aromatic hydrocarbons. It has been exploited to great advantage on a number of cyclometalated complexes of Pt(II) and Pd(II) that are related

* To whom correspondence should be addressed. E-mail: joseph.deaton@kodak.com. Phone: 585-477-9651. Fax: 585-588-7611. Eastman Kodak Company, 1999 Lake Ave., Rochester, NY 14650-2103.
[†] Eastman Kodak Company, Retired.
[‡] Eastman Kodak Company.
[§] University of Rochester.

10.1021/jp056225j CCC: $33.50
Published on Web 07/21/2006

CHART 1: IrL_2acac Compounds of This Study[a]

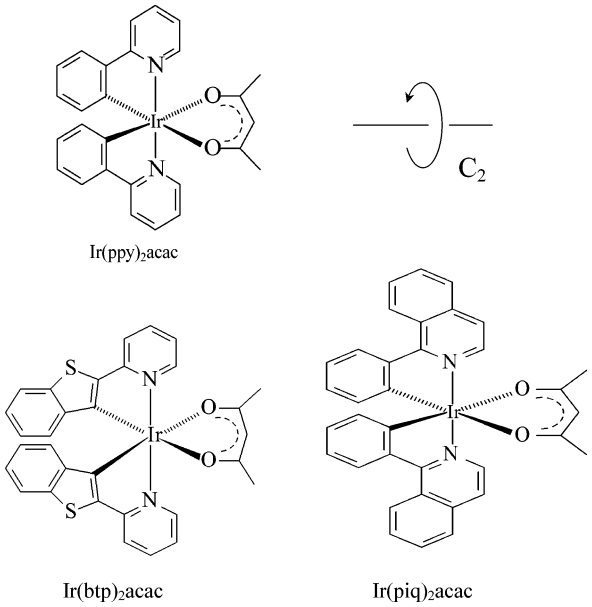

[a] All have a two-fold axis of symmetry (C_2) as illustrated for $Ir(ppy)_2acac$.

to the Ir(III) complexes of interest for OLED applications.[24] In the work reported here, we have examined the emission, excitation, and Zeeman spectra of the IrL_2acac complexes and, briefly, two of the corresponding IrL_3 complexes in a Shpol'skii matrix. The IrL_2acac complexes produce surprisingly good Shpol'skii spectra from which we have extracted parameters characterizing the individual triplet sublevels. The IrL_3 complexes also show limited narrow-line spectra which we have not yet attempted to analyze.

Broadband spectra in a disordered host—typically a glass-forming solvent or a polymer—usually have relatively low information content. It has been discovered recently that $Ir(ppy)_3$ in frozen tetrahydrofuran (THF) is a striking exception.[27] The three sublevels of the lowest triplet manifold have very different rate constants for decay, significantly different spectra, and a spread of energies that is large enough that their relative populations can be changed drastically by varying the temperature. Thus, it has been possible to analyze the decay kinetics in this broadband system to obtain the relative energies and the decay rates for the individual sublevels, even though the separation of the sublevels ($\approx$100 cm^{-1} or less) is far smaller than the resolution of the spectral bands. In the present study, we have also investigated the spectra and decay kinetics of the IrL_2acac complexes in a polymeric host, poly(methyl methacrylate) (PMMA). The combined results from the narrow-line and the broadband spectra allow us to extract a nearly complete set of radiative and nonradiative rate constants and broadband spectra for the individual triplet sublevels.

The present study was undertaken as a preliminary exploration of what could be learned from the Shpol'skii and broadband spectra. It is hoped that the present results will stimulate further work on these fascinating and technologically important materials.

2. Experimental Section

The complexes *fac*-tris(2-phenylpyridinato-N,C^2)iridium(III) [$Ir(ppy)_3$], bis(2-phenylpyridinato-N,C^2)iridium(III) acetylacetonate [$Ir(ppy)_2acac$], and bis(2-(2′-benzothienyl)pyridinato-$N,C^{3'}$)-iridium(III) acetylacetonate [$Ir(btp)_2acac$] were synthesized by modifications to procedures in ref 9. Bis(1-phenylisoquinolinato-$N,C^{2'}$)iridium(III) acetylacetonate [$Ir(piq)_2acac$] was synthesized by a modification to the procedure in ref 45, and *fac*-tris(1-phenylisoquinolinato-$N,C^{2'}$)iridium(III) by the procedure in ref 46. Molecular structure determination by single-crystal X-ray diffraction (results to be reported elsewhere) confirmed that $Ir(piq)_2acac$ has a *cis*-C,C′-*trans*-N,N′ geometry analogous to that reported for $Ir(ppy)_2acac$ and inferred for $Ir(btp)_2acac$ by NMR studies (ref 9; see Chart 1).

Solutions in *n*-octane were prepared by dissolving the complexes with heat and stirring. The solutions were allowed to stand for one or more days, and no precipitation was observed. The concentrations were on the order of 10−40 μM. PMMA films were made by dissolving the complexes in dichloromethane containing 10% PMMA and blade coating on poly(ethylene terephthalate) (PET) sheets. The loadings in the films were ca. 1 wt %, corresponding to concentrations of ca. 20 mM.

The experimental apparatus has been described elsewhere.[47] A sample is cooled in a gas-flow liquid helium cryostat to 6 K. Temperatures between 6 and 290 K are obtained by controlling the He flow and the heater current on the sample block. Temperature measurement and control make use of a thermistor mounted on the sample holder. Temperatures below 4 K are obtained by allowing the sample chamber to fill with liquid He and reducing the pressure and are evaluated accurately from the vapor pressure of the helium. For steady-state emission scans, excitation is provided by a helium−cadmium laser operating at 325 or 442 nm or an argon-ion laser operating at 351/364 or 458 nm. Low-resolution steady-state excitation scans are obtained using a 150 W xenon lamp and 0.19 m monochromator. High-resolution excitation spectra are obtained using a tunable dye laser. In most cases, emission is optically chopped and directed into a 0.75 m monochromator, detected with a photomultiplier tube, and measured with a lock-in amplifier. In some cases emission spectra are obtained with a free-running, gated photon counter. Control experiments using rubrene in PMMA as a standard have established that measurements of the relative intensity at various temperatures are accurate to $\pm$10% or better. In each case, a minor contribution from the PET substrate to the emission in PMMA is subtracted before analysis. The magnitude of this contribution serves as a further check on the precision of the intensity measurements.

For Zeeman emission experiments, the sample is placed inside a split-coil superconducting magnet immersed in liquid helium in a double metal Dewar, which provides fields up to 3 T (30 kG). Sample temperatures down to 1.7 K are again obtained by lowering the vapor pressure of the liquid helium.

Excited-state lifetimes in *n*-octane are measured using a Nd:YAG laser, frequency tripled to 355 nm with a $\sim$5 ns pulse width. Lifetimes in PMMA are measured using a $\sim$480 nm dye laser pumped by the same frequency-tripled laser. Decay profiles are recorded using a load resistor, preamplifier, and digital oscilloscope. Emission spectra are also obtained at various delay times with a gated photon counter. In all spectroscopic measurements, scan control and data acquisition are accomplished through a computer interface.

As discussed below, the decay profiles in PMMA are frequently nonexponential. Various artifactual explanations have been ruled out. The decay profiles are not affected by the intensity of the exciting pulse (i.e., not influenced by heating of the sample), the wavelength of excitation (355 or 480 nm), or the choice of cutoff filter used to shield the monochromator from scattered excitation light. Virtually identical decays are observed with different concentrations of the complex (i.e.,

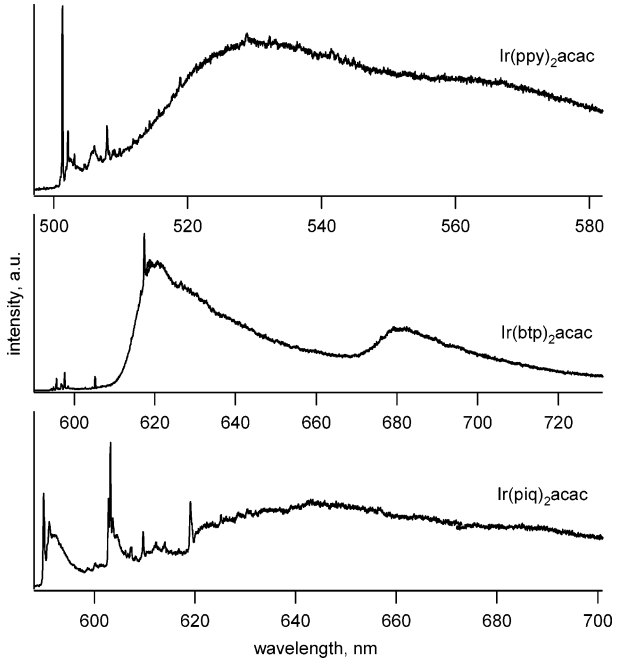

Figure 1. Survey emission spectra of the IrL_2acac complexes in *n*-octane at 5 K. Excitation was at 442 nm; essentially the same spectra were observed with 351/364 nm excitation. These spectra are actually composites of three or more sequential scans of about 1000 points.

energy transfer and/or solute aggregation do not appear to be factors), with films immersed in liquid nitrogen (i.e., at a very uniform temperature), and with frozen solutions in THF. The response of the detection electronics was checked by verifying that the decay profile for $Ir(ppy)_3$ in N_2-purged THF at room temperature is, as anticipated, cleanly exponential.

3. Narrow-Line Emission in *n*-Octane: Results and Analysis

Survey emission spectra of the IrL_2acac complexes (L = ppy, btp, piq) in *n*-octane at 5 K are shown in Figure 1. Each has been reproduced several times. Each exhibits numerous sharp lines superimposed on a broad background. The sharp lines are not substantially affected by variations in the exciting wavelength (351/364 or 442 nm), whereas the broad components are more variable. As discussed below, each spectrum exhibits two or more 0−0 bands associated with different molecular sites with varying intensities that reflect their relative populations. Each spectrum further exhibits at least 25 vibronic bands, distributed over the first 2500 cm^{-1} from the 0−0 bands, and usually associated with the most intense 0−0 band. The resolution of these Shpol'skii spectra is much higher than is possible with normal glass-forming hosts (see, for instance, Figures 7−9 below). The spectrum of $Ir(ppy)_3$ in *n*-octane (not shown) exhibits a few weak, but sharp, lines starting at about 505 nm. Well-resolved spectra were obtained for $Ir(piq)_3$ in *n*-octane with about a dozen sharp lines, starting at 613.5 nm, indicating the presence of several sites. The spectrum of $Ir(btp)_3$ in *n*-octane was not investigated.

The sharp-line components in a Shpol'skii spectrum represent guest molecules in a limited number of specific sites that correspond to a few specific ways in which the host can pack around a guest. The phenomenon is most often observed with planar guest molecules, and it is remarkable that it occurs with the present nonplanar Ir complexes (Chart 1). To some degree, the underlying broad emission resembles that in a typical glassy host. It varied from experiment to experiment (cf. Figure 2),

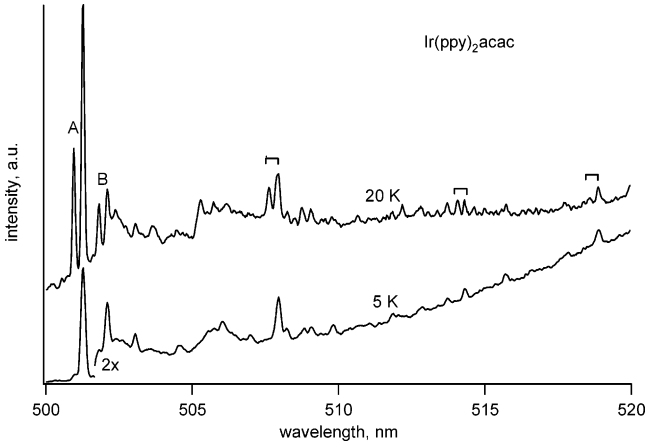

Figure 2. Expanded view of the spectrum of $Ir(ppy)_2acac$ in *n*-octane at 5 and 20 K. Excitation was at 442 nm and 351/364 nm, respectively. The two spectra represent different samples and are normalized independently. Two sites are identified and labeled A and B. Many pairs of vibronic lines (bracketed) exhibit approximately the same separation and the same pattern of temperature-dependent intensity as observed at the site origins. The different intensity of the broad background in the two spectra illustrates the variability of that component.

indicating that it belongs to a separate component of the sample, rather than a congestion of narrow lines. Underlying broad components were also observed in some of the Shpol'skii spectra of Pd and Pt complexes and attributed to dimers and higher aggregates.[24] For the present Ir complexes, the broad components might also be due to aggregates. Alternatively, perhaps the packing around a nonplanar Ir complex is less effective in stabilizing the preferred arrangements of guest and host (discrete sites), relative to a quasi-continuum of alternative structures. The resulting inhomogeneously broadened emission could be responsible for the broad component of the spectra.

Figure 2 shows the region near several electronic origins in more detail for the case of $Ir(ppy)_2acac$ at 5 and 20 K. Figures 3−5 show further expanded spectra in the origin region for each complex at two or three temperatures. In each case, the relative prominence of different lines varies with the temperature. The changing intensity patterns are attributed to changing populations of the triplet sublevels at each site, and this information was used to help identify emission lines with different sublevels and different sites. Excitation spectra, such as illustrated in Figure 4, also were used in the analysis. The intensity patterns indicate that the different triplet substates have very different oscillator strengths in their 0−0 bands.

As an example, in Figure 3, the lines at 500.85 and 501.17 nm appear to originate from $Ir(ppy)_2acac$ molecules in the same site (site A) and represent the 0−0 bands of two of the three triplet sublevels (A_1, A_2). The lines at 501.71 and 501.97 nm exhibit approximately the same relative intensities as a function of temperature, and they are assigned to a second site (B). The modest differences in intensity ratios at the higher temperatures are consistent with the slightly different level splittings for sites A and B—13 and 10 cm^{-1}, respectively. The line at 501.27 nm probably represents the lowest sublevel of a third, relatively minor, site with the higher sublevel hidden under the prominent A_1 line. For $Ir(ppy)_2acac$, no third sublevel has been observed up to 40 K. However, at 30 K and above, the spectra of $Ir(btp)_2acac$ and $Ir(piq)_2acac$ exhibit an additional weak emission line that was identified as a third sublevel (615.52 nm for $Ir(btp)_2acac$ site E_3, Figure 4). For $Ir(btp)_2acac$, this assignment was confirmed by an excitation spectrum (topmost curve, Figure 4) that shows both the corresponding line (E_3) and another at

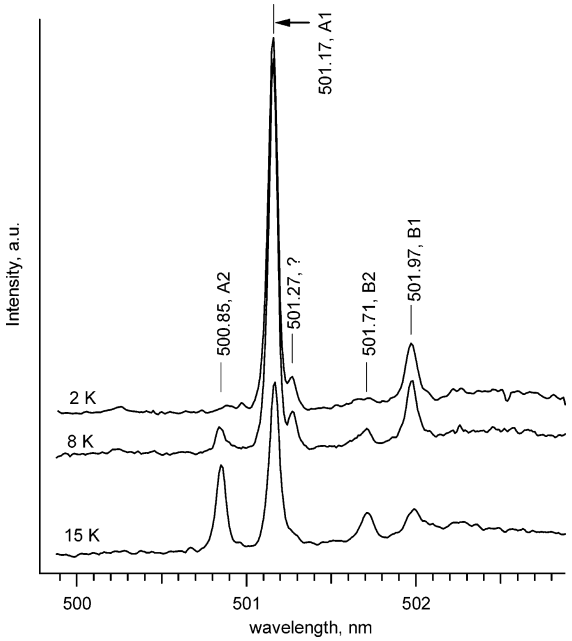

Figure 3. High-resolution emission spectra of Ir(ppy)$_2$acac at 2, 8, and 15 K in the region of the 0−0 bands of the more prominent sites in *n*-octane (A, B). The line at 501.27 nm probably belongs to another, minor site. Excitation was at 351/364 nm. The spectra have been normalized independently.

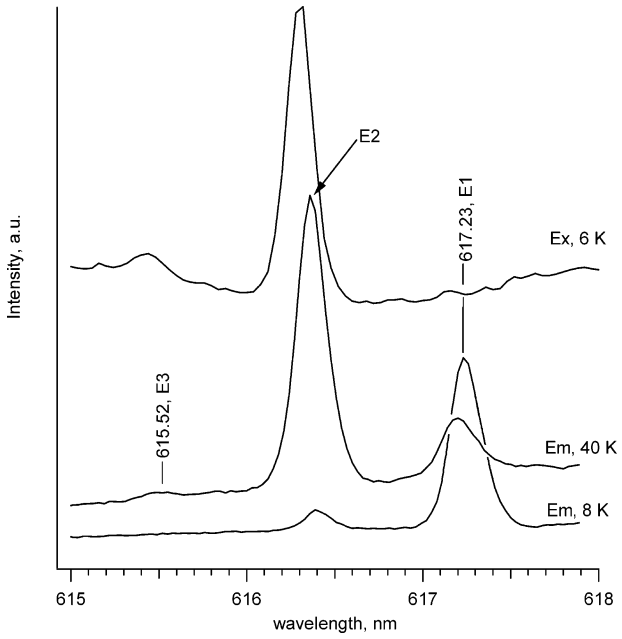

Figure 4. High-resolution spectra of Ir(btp)$_2$acac in *n*-octane in the region of the 0−0 bands of the prominent lowest energy site: emission spectra at 8 and ≈40 K with excitation at 351/364 nm; excitation spectrum at 6 K with detection at 676.04 nm. The line marked E_2 is shifted slightly from its wavelength at 8 K (616.39 nm). The spectra have been normalized independently.

616.30 nm (E_2). Thus, both lines belong to the same site (E). (The feature at ≈617.28 nm, though very weak, appeared in each of several excitation spectra. It is most likely E_1, consistent the present assignments.) The detection wavelength, 676.04 nm, is evidently a vibronic sideband belonging to the same site. For the weaker but higher energy sites of Ir(btp)$_2$acac A, B, and D, excitation spectra indicate that the A_2, B_2, and D_2 lines arise from distinct sites. For Ir(piq)$_2$acac, a single excitation line observed at 587.88 nm corresponds to sublevel 3 of site A. Apparently this sublevel has much the largest oscillator strength.

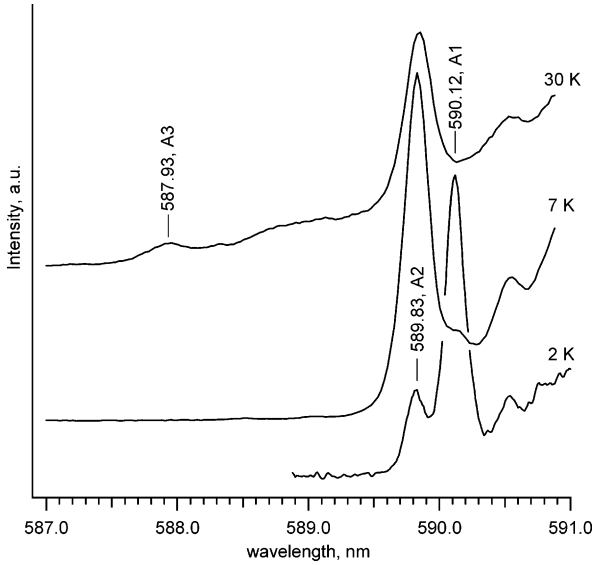

Figure 5. High-resolution emission spectra of Ir(piq)$_2$acac in *n*-octane at 2, 7, and ≈30 K in the region of the 0−0 bands of the most prominent site. Excitation was at 351/364 nm. The spectra have been normalized independently.

Characteristics of the 0−0 bands of the triplet sublevels of prominent sites are given in Table 1 for the three IrL$_2$acac complexes. The sublevels at each site are indexed in order of increasing energy. Ratios of oscillator strengths (f_1, f_2, f_3) were estimated from the integrated intensities of select spectra. For emission spectra, it was assumed that the sublevels were populated according to a Boltzmann distribution. It was further assumed that any differences in polarization would have little effect because the media were highly turbid. The relative oscillator strengths reported in Table 1 reveal strikingly different ratios for the three compounds.

The line widths (fwhm) of the 0−0 bands in emission are 4.0 cm^{-1} for Ir(ppy)$_2$acac, 6.3 cm^{-1} for Ir(btp)$_2$acac, and 6.0 cm^{-1} for Ir(piq)$_2$acac at 2 K, and they increase only slightly up to 30 or 40 K. An uncertainty broadening of this magnitude would imply a lifetime of 1 or 2 ps ($\Delta t = \hbar/\Delta E$). The lifetime of the triplet manifold at liquid helium temperatures is ∼50 μs or greater (see Table 2, below). The lifetime of the individual sublevels, however, is determined by spin−lattice relaxation (SLR; see below) and is considerably shorter. Literature values for the rate of SLR in similar complexes at 2 K are ca. 2×10^6 s^{-1},[24] much too slow to account for the observed line widths. Moreover, with uncertainty broadening, a higher sublevel should have a broader emission than a lower, and the breadths should be strongly temperature-dependent.[24] Neither effect is observed. Evidently, the lines are inhomogeneously broadened, perhaps as a consequence of nonuniform mechanical strain effects in this polycrystalline matrix. In fact, in the case of Ir(btp)$_2$acac (see Figure 4), specific laser excitation at the energy of E_2 produced a narrower emission (≈2 cm^{-1} fwhm) from E_1 than was observed with excitation at 442 nm, presumably as a result of site selection within the already narrow distribution of site E. The vibronic sidebands tend to be somewhat wider (≈10 cm^{-1}); and, conversely, the greater width of some lines was used to assign them tentatively as vibronic sidebands of some origin. An example of a probable vibronic sideband is the intense line at 603 nm in the spectrum of Ir(piq)$_2$acac, Figure 1.

The effect of a magnetic field on the A_1 origin of Ir(piq)$_2$-acac at 1.7 K is shown in Figure 6. At 3 T (30 kG), the intensity increases more than 3-fold, the line shifts to lower energies by ca. 0.6 cm^{-1}, and the fwhm increases by 1.1 cm^{-1}, relative to

TABLE 1: Characteristics of the 0−0 Bands Representing Prominent Sites in the Shpol'skii Emission Spectra of Three Ir Complexes at 8 K, Except as Noted[a]

wavelength, nm[b] (intensity[c])	energy,[d] cm^{-1}	assignment	relative energy,[e] cm^{-1}	rel oscillator strengths[f]
		$Ir(ppy)_2acac$		
500.85 (m)	19961	A_2	13	$f_2/f_1 = 1.5$
501.17 (s)	19948	A_1	0	(site A, 15 K)
501.71 (w)	19926	B_2	10	
501.97 (m)	19916	B_1	0	
		$Ir(btp)_2acac$		
593.40 (w)	16848	A_2	26	
594.30 (w)	16822	A_1	0	
594.70 (w)	16811	B_2	23	
595.50 (m)	16788	B_1	0	
596.74 (m)	16753	C_2	22	
597.54 (m)	16731	C_1	0	
604.37 (w)	16542	D_2	19	
605.06 (m)	16523	D_1	0	
615.52 (vw)[g]	16242	E_3	45	
616.44 (s)	16219	E_2	22	
617.23 (m)	16197	E_1	0	
615.58 (w)[h]	16241	E_3	∼45	$f_3/f_2 = 0.07$
616.42 (s)[h]	16218	E_2	∼22	$f_2/f_1 = 56$
≈**617.28** (vw)[h]	∼16196	E_1	0	(site E, 6 K)
		$Ir(piq)_2acac$		
587.93 (vw)[g]	17004	A_3	63	$f_2/f_1 = 120 \pm 40$
589.83 (s)	16950	A_2	9	(site A, 2 K)
590.12 (w)	16941	A_1	0	
587.88[h] (m)	17006	A_3	65	$f_3/f_2 \geq 20$
590.94 (m)	16918	B_2	8	(site A, 6 K)
591.22 (w)	16910	B_1	0	

[a] The excitation wavelength was either 351/364 or 442 nm. [b] Wavelengths in bold are from an excitation spectrum. Not corrected to vacuum. [c] s = strong, m = medium, w = weak, vw = very weak. [d] Wavenumbers corrected to vacuum. Uncertainties are ∼1 cm^{-1}. [e] Energy above the lowest triplet sublevel at the same site. Uncertainties are <1 cm^{-1}. [f] Evaluated at temperature indicated in parentheses. [g] At 30 K. [h] At 6 K.

TABLE 2: Lifetime Data for IrL_2acac Complexes in *n*-Octane[a]

site	temp, K	lifetime, μs
	$Ir(ppy)_2acac$	
A_1	1.7, 1.9	59
	4.2	56
	$Ir(btp)_2acac$	
E_1	1.9	88
	4.2	76
	20	35
E_2	20	38
	$Ir(piq)_2acac$	
A_1	1.7−2.0	79
	4.2	48
	6	51
A_2	1.7, 1.9	70
	4.2	48

[a] The uncertainties are ±5% or less.

the values at zero field. For $Ir(ppy)_2acac$ at 3 T and 1.7 K (not shown), the stronger origin (A_1) exhibits no significant change in intensity, but it shifts by ≈0.5 cm^{-1} to lower energies, whereas the fwhm increases somewhat (≈0.4 cm^{-1}). Magnetic-field effects on $Ir(btp)_2acac$ were not investigated. The effects observed for $Ir(piq)_2acac$ and $Ir(ppy)_2acac$ are consistent with the assigned site origins and, in particular, with the separation and relative oscillator strengths of the lower two origins at each site. At 3 T, the Zeeman matrix element (H_{ij}) coupling two sublevels (i, j), ranges up to 3 cm^{-1}, depending on the orientation

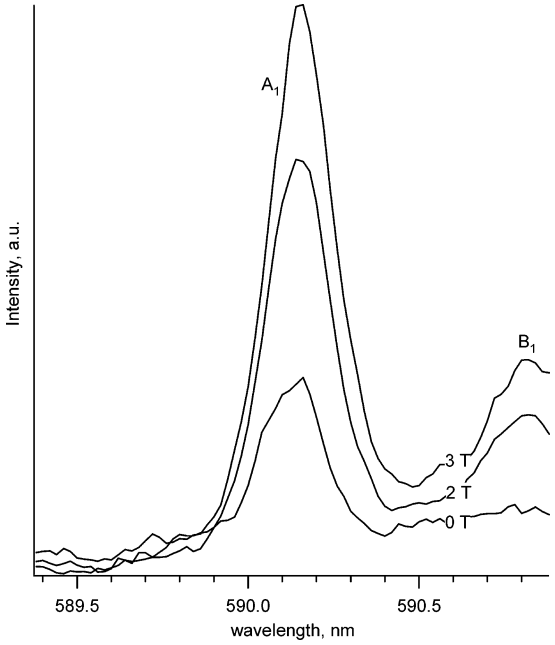

Figure 6. High-resolution emission spectra of $Ir(piq)_2acac$ at magnetic fields of 0, 2, and 3 T at 1.7 K. The arbitrary units are the same for each spectrum. The excitation wavelength was 442 nm. The two origins, A_1 and B_1, show similar, large increases in intensity at high fields. The A_1 line also shifts 0.6 cm^{-1} bathochromically and broadens by about 1 cm^{-1}.

of the magnetic field in molecule-fixed axes and assuming a *g*-factor of 2.[48,49] This value is a sizable fraction of the splitting between the lower two sublevels (Δ). Therefore, a substantial mixing of the lowest sublevel with one or both of the other sublevels must occur. In $Ir(piq)_2acac$, where the higher sublevels have a much greater oscillator strength in their 0−0 bands, this mixing can easily increase the intensity of the lowest origin, as observed. In $Ir(ppy)_2acac$, the oscillator strengths of the lowest and middle origins are similar, so it is not particularly surprising that no intensity effect was detected. For the lowest sublevel, at any orientation, the shift should be negative and of magnitude $\sim|H_{12}|^2/\Delta \sim 1$ cm^{-1}. The angular average of this shift should be somewhat smaller, consistent with the ∼0.5 cm^{-1} shifts observed. The line width effects, though small, are somewhat larger than might be expected, given that the width (strictly, the rms width, σ) in the presence of a magnetic field should be given by $\sigma = (\sigma_0^2 + \sigma_B^2)^{1/2}$, where σ_0 is the line width at zero field, and σ_B is the width of the distribution of Zeeman shifts. However, because the line shape represents an average of energies weighted by orientation-dependent intensities, a quantitative explanation of the shifts and line widths must wait for a determination of the polarizations of the emissions from the individual sublevels.[50]

For all three complexes, the vibronic sidebands are individually weak and exhibit no recognizable progressions. The only strong vibrational sidebands are two pairs of fairly strong bands for $Ir(piq)_2acac$, one pair located at about 603 nm (363 and 365 cm^{-1} below each of origins A_1 and A_2) and the other at about 619 nm (798 cm^{-1} below the respective origins). The underlying broad components, as well as the broadband spectra discussed later, exhibit moderately intense sidebands in the C−C stretch region (ca. 1400 cm^{-1}). The corresponding vibronic activity in the Shpol'skii spectra appears to be distributed over numerous modes, none of which is individually very strong. Nevertheless, their collective intensity relative to the intensity of the 0−0 bands is consistent with the intensity ratios in the broad spectra. It appears that the ground and excited states have very similar

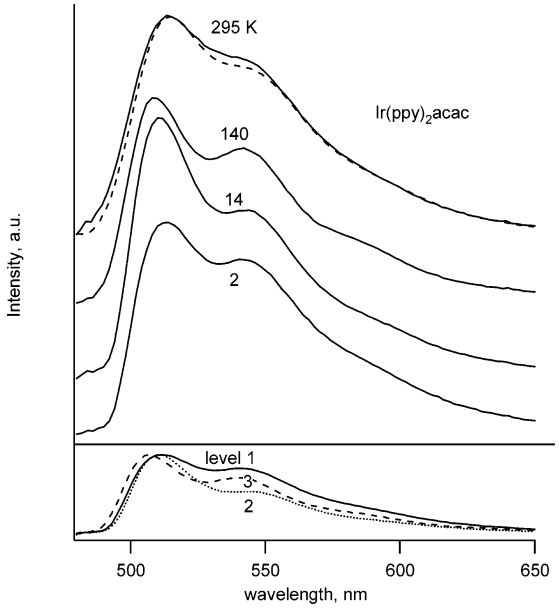

Figure 7. Emission spectra of $Ir(ppy)_2acac$ in PMMA excited at 458 nm. Upper panel: observed spectra at various temperatures (solid curves) and predicted spectrum at 295 K (dashed curve). Relative intensities are accurate to about 10%. Lower panel: spectra of individual sublevels, normalized, as evaluated from observed spectra at 2, 7, 14, 28, and 50 K. Actual intensity of sublevel i is proportional to $k_{r,i}$ (see Table 3).

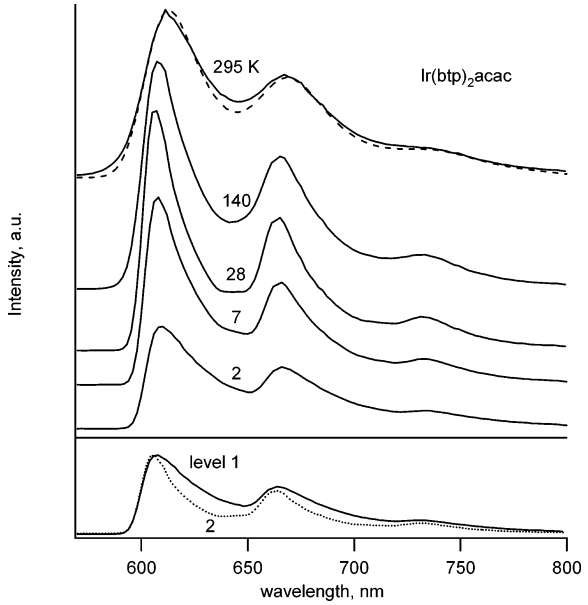

Figure 8. Emission spectra of $Ir(btp)_2acac$ in PMMA excited at 458 nm. Upper panel: observed spectra at various temperatures (solid curves) and predicted spectrum at 295 K (dashed curve). Relative intensities are accurate to about 10%. Lower panel: spectra of the lower two sublevels, normalized, as evaluated from observed spectra at 2 and 50 K. Actual intensity of sublevel i is proportional to $k_{r,i}$ (Table 3).

geometries and potential-energy surfaces. Metal−ligand vibrational frequencies are generally below 500 cm^{-1},[24,25] and several corresponding bands are observable in the spectra. In most of the spectra, there are also slightly broadened lines that peak 30−50 cm^{-1} below the 0−0 bands of the stronger sites. These bands are assigned to matrix (*n*-octane) lattice modes.[41] In the absence of strong progressions, assignments to vibrational sidebands are tentative. They could be confirmed by excitation spectra, as illustrated above with the 676.04 nm detection band in $Ir(btp)_2acac$, or by ground-state vibrational data.

Excited-state lifetimes observed for several sites and sublevels are listed in Table 2. Most of the entries represent repeated measurements, and their reproducibility was better than ±5%. In each case, the decay was a single exponential, although a short-lived component might be hidden by the RC time constant of ∼5 μs used with these slow decays. In each case, the decay was faster at 4.2 K than at 2 K and particularly so for $Ir(piq)_2acac$, which has the smallest splitting between the lower two sublevels. When both lower sublevels could be observed, they exhibited the same lifetime, indicating that equilibration between the levels (SLR) is fast, relative to the excited-state lifetime even at 2−4 K. For the three complexes at 2 and 4.2 K, spectra obtained over the first 10 μs, and delayed by 50 μs after excitation, exhibited the same intensity pattern, again consistent with relatively fast SLR.[24]

4. Broadband Emission in PMMA: Results and Analysis

Figures 7−9 display emission spectra of the three IrL_2acac compounds, dissolved in PMMA, at selected temperatures from 2 to 295 K. In each case, the overall intensity of the spectrum increases with increasing temperature—modestly for $Ir(ppy)_2acac$ and dramatically for $Ir(btp)_2acac$ and $Ir(piq)_2acac$. It is common for an emission to become weaker as the temperature is increased because nonradiative decay pathways become more competitive,[18,25] but these compounds exhibit the opposite trend. The band shapes also change, moderately for $Ir(ppy)_2acac$ and

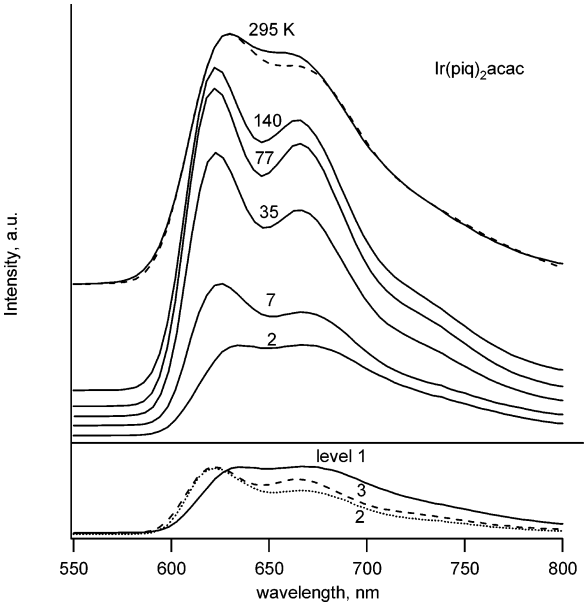

Figure 9. Emission spectra of $Ir(piq)_2acac$ in PMMA excited at 458 nm. Upper panel: observed spectra at various temperatures (solid curves) and predicted spectrum at 295 K (dashed curve). Relative intensities are accurate to about 10%. Lower panel: spectra of individual sublevels, normalized, as evaluated from observed spectra at 2, 7, and 35 K. Actual intensity of sublevel i is proportional to $k_{r,i}$ (Table 3).

$Ir(btp)_2acac$ and dramatically for $Ir(piq)_2acac$. It is common for spectra to exhibit more poorly resolved peaks as the temperature increases, but these compounds exhibit the opposite trend except at the highest temperatures. Similar behavior has been reported previously for $Ir(ppy)_3$ and will be discussed below.[27]

Lifetime data are shown in Figure 10 as inverse lifetimes or decay rates (strictly, rate constants, k) as functions of temperature. For each compound, the luminescence transient exhibits an exponential decay at the lowest and the highest temperatures, but markedly nonexponential in an intermediate range where the lifetime is most strongly temperature-dependent (e.g., 20−

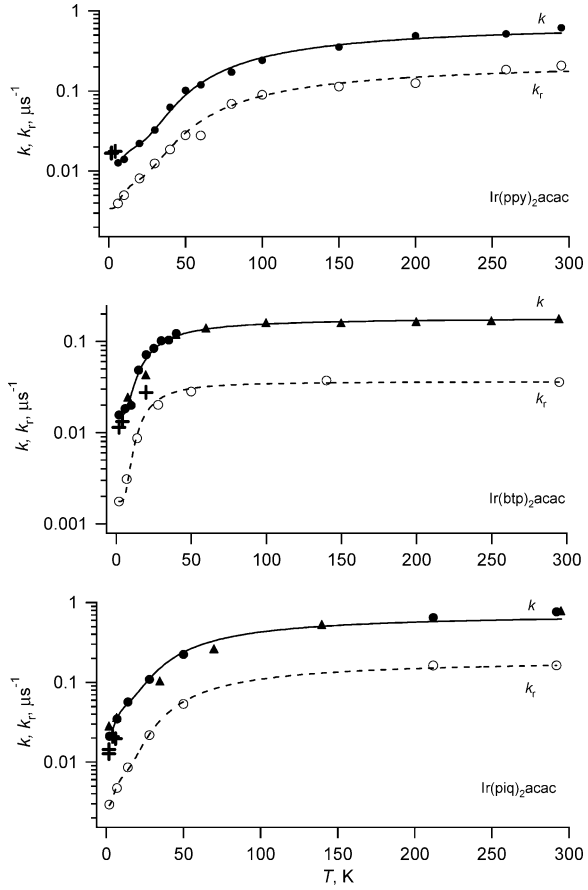

Figure 10. Effective excited-state decay rates (inverse lifetimes, k, solid and "+" symbols) and radiative decay rates (k_r, open symbols) for IrL_2acac complexes in PMMA (circles, triangles), and *n*-octane ("+" symbols). Circles and triangles represent different data sets. Some points for *n*-octane represent averages over 2−4 measurements. Excitation in PMMA was at ∼480 nm (circles) or 355 nm (triangles); excitation in *n*-octane was at 355 nm. Curves are fits to data in PMMA using eq 1 with parameters indicated in Table 3.

50 K for $Ir(ppy)_2acac$). The cause of this behavior is under investigation. To indicate the temperature dependences in such a case, the data point in Figure 10 is an effective rate constant calculated by dividing the integral of the luminescence transient into the initial intensity. (As a measure of the nonexponentiality, if the initial slope of the decay were used instead, the resulting "initial decay rate" would have been 30% larger in the few, most severe cases.) The lifetimes decrease dramatically with increasing temperature, as is often the case, but the increasing intensity of the emission points to a rather unusual reason: The decay rates increase rapidly with increasing temperature, but evidently, the *radiative* decay rates (k_r; see below) increase even more rapidly. For comparison, data in the *n*-octane are included in Figure 10. The differences between the two hosts, with faster decays in PMMA in two cases and slower in the third, suggest a surprising sensitivity of this electronic property to the molecular environment. The differences do not appear to be an artifact of using effective lifetimes, when necessary, because some of those decays are very nearly monoexponential at the lowest temperatures. Perhaps the nonexponential decays are a disorder phenomenon that is enabled by the sensitivity to the environment.

Even at the lowest temperatures, it appears that SLR is considerably faster than the overall decay of the luminescence, as is commonly the case for similar heavy-metal complexes.[24] For instance, as discussed below, the three sublevels have different rate constants for decay, and different spectra (Figures 7−9). Therefore, at temperatures where more than one sublevel contributes significantly to the emission, slow SLR should result in a wavelength-dependent decay profile. No such dependence was observed for $Ir(piq)_2acac$ at temperatures and wavelengths chosen to accentuate the effect (2−50 K; 620, 635, and 680 nm). Fast SLR is a prerequisite for the use of the thermal averages below. For the lifetimes approaching 100 μs, it is still possible that a short period of equilibration among the magnetic sublevels could be hidden by the instrumental time constant of ∼5 μs used with these lifetimes.

TABLE 3: Properties of the Individual Magnetic Sublevels for IrL_2acac Complexes in PMMA[a]

parameter	level	$Ir(ppy)_2acac$	$Ir(btp)_2acac$	$Ir(piq)_2acac$
E_i, cm^{-1}	1	0	0	0
	2	13	24	9
	3	103	45	63
k_i, μs^{-1}	1	0.010	0.015	0.021
	2	0.047	0.30−0.45	0.13
	3	2.1	0.20−0.05	2.1
$k_{r,i}$ (rel)	1	1	1	1
	2	4.9,[b] 5.5,[b,c] 5.1,[d] 4.9[e]	54,[b] 57[e]	10,[b] 6.5,[d] 7.2[e]
	3	220,[b] 190,[b,c] 180,[d] 220[e]	4	270,[b] 200,[d] 270[e]
$k_{r,i}$, μs^{-1}	1	0.0034[d]	0.0018	0.0028[d]
	2	0.018[d]	0.100	0.019[d]
	3	0.70[d]	0.007	0.57[d]
$k_{nr,i}$, μs^{-1}	1	0.0070	0.013	0.018
	2	0.030	0.20−0.25	0.11
	3	1.4	0.19−0.04	1.5
Φ_i	1	0.34	0.11	0.14
	2	0.38	0.3−0.2	0.14
	3	0.30	0.04−0.15	0.27
		Reference Data at ∼295 K		
k (PMMA, μs^{-1})		0.61	0.18	0.79
k (soln)		0.62[f]	0.17[f]	
Φ (soln)		0.34[f]	0.21[f]	0.21[g]

[a] Energies (E_i), relative to lowest level; decay rates (inverse lifetimes, k_i); radiative and nonradiative rates ($k_{r,i}$ and $k_{nr,i}$); and ratios $\Phi_i = k_{r,i}/k_i$. Parameters in italics were fixed at values obtained in *n*-octane. Assumptions required to evaluate $k_{r,i}$ and $k_{nr,i}$ are detailed in the text. Additional room-temperature data used to determine the absolute radiative and nonradiative rates: decay rates (inverse lifetimes, k) and quantum efficiencies (Φ) of emission in PMMA and in the solvents indicated. [b] From integrated spectra of individual sublevels evaluated at ≤50 K. [c] Steady-state intensities were corrected for polarization bias. [d] From amplitudes of decay transients. [e] From integrals of observed spectra at all temperatures. [f] In 2-methyltetrahydrofuran (refs 9 and 10). [g] From relative quantum efficiencies of $Ir(piq)_2acac$ and $Ir(ppy)_2acac$ in toluene and absolute efficiency for $Ir(ppy)_2acac$ in 2-methyltetrahydrofuran (ref 9).

We turn now to a more quantitative analysis of the decay rates and the spectra. If it is assumed that the individual magnetic sublevels ($i = 1-3$) have characteristic decay rates that are independent of temperature (k_i), the observed rate k should be a thermal average,[28,31,51,52]

$$k = \sum_i k_i \exp(-\beta E_i) / \sum_i \exp(-\beta E_i) \qquad (1)$$

where $\beta^{-1} = k_B T$ is the thermal energy and E_i is the energy of sublevel i. The data in Figure 10 for each complex were fit to eq 1 by taking the level splittings obtained in *n*-octane as known and adjusting the remaining parameters. For $Ir(ppy)_2acac$, the unknown position of the third sublevel was also an adjustable parameter. The resulting, rather encouraging, fits are shown as solid curves, and the parameters are indicated in Table 3. In the case of $Ir(btp)_2acac$, the fact that k is nearly constant above 50 K makes it difficult to evaluate k_2 and k_3 individually, though $k_2 + k_3$ is well determined. Values (k_2, k_3) ranging from (0.3, 0.2) to (0.45, 0.05) fit the data acceptably. Given the somewhat different decay rates observed in PMMA and *n*-octane, the use

of energy levels from *n*-octane as fixed parameters is somewhat tentative. Nevertheless, the fitting parameters do not depend strongly on the assumed level splittings. For instance, in the case of $Ir(ppy)_2acac$, virtually the same k_i values (within ±10%) and third sublevel energy (within 3 cm^{-1}) were obtained using the splittings obtained from two different Shpol'skii sites (10 and 13 cm^{-1}). For different reasons (see below), the assumption of temperature-independent k_i is also tentative, and the parameter values must be taken as rough estimates. Even so, they display some remarkable trends, which will be discussed later. It should be mentioned that a rather different model, involving just two triplet levels separated by a small energy barrier (~100 cm^{-1}), has been proposed to explain the temperature dependence of the lifetimes for $Ir(ppy)_3$ in PMMA.[20]

Radiative rate constants (k_r) for $Ir(ppy)_2acac$ and $Ir(piq)_2acac$ were evaluated from the amplitude of the time-resolved phosphorescence signal, i.e., the intensity immediately after the excitation pulse. Let $I(\lambda)$ be the unimolecular rate constant for emission into a 1-nm spectral range ($\lambda \pm 0.5$ nm) and λ_d be the wavelength of detection. The measured amplitude is jointly proportional to (a) this $I(\lambda_d)$, (b) the number of molecules excited by the laser pulse, and (c) the sensitivity of the detection system. The absorption spectra in homogeneous media are broad,[9,10,20] and the excitation conditions were kept constant throughout each experiment except for occasional adjustments of the excitation intensity. Thus, it is safe to assume that factors (b) and (c) were otherwise constant, and the observed amplitudes should be simply proportional to $I(\lambda_d)$. The quantity of interest, k_r, is the integral of $I(\lambda)$ over the entire spectrum. The conversion factor $k_r/I(\lambda_d)$, which depends somewhat on temperature, was evaluated from steady-state spectra. Observed amplitudes were multiplied by this factor to give a quantity proportional to k_r at each temperature. An alternative procedure was used for $Ir(btp)_2acac$, because the amplitude data were not sufficiently accurate. Each emission spectrum was integrated, to obtain a relative quantum efficiency, and multiplied by the value of k at the same temperature to obtain a quantity proportional to k_r. This use of an effective rate constant is justified if the emission spectrum in the transient experiment does not change with time.

The proportionality constant required to set the radiative rates on an absolute scale was evaluated from the measured inverse lifetime (k) and quantum efficiency (Φ) at room temperature. Literature values of Φ in 2-methyltetrahydrofuran solution were used for $Ir(ppy)_2acac$ and $Ir(btp)_2acac$ because the corresponding excited-state lifetimes were identical to those measured here in PMMA (see Table 3). For $Ir(piq)_2acac$, the efficiency relative to that for $Ir(ppy)_2acac$ was measured in a toluene solution and combined with the literature value of Φ for the latter in 2-methyltetrahydrofuran. It is again assumed that the value of Φ in PMMA is the same as in fluid solution.

Assuming that each triplet sublevel has its own radiative rate constant $k_{r,i}$, independent of temperature, the $k_{r,i}$ were evaluated from the temperature dependence of the observed radiative rates. It is assumed that Boltzmann equilibrium is established among the triplet sublevels at each temperature, and the dependence of k_r on temperature was analyzed using eq 1 with k and k_i replaced by k_r and $k_{r,i}$. In the case of $Ir(btp)_2acac$, the near constancy above 50 K again made it impossible to determine $k_{r,2}$ and $k_{r,3}$ individually, so the ratio of the two was equated to f_3/f_2 in *n*-octane and the magnitudes of $k_{r,2}$ and $k_{r,3}$ were determined together. The resulting fits are shown in Figure 10 (dashed curves), and the parameters are listed in Table 3. Also tabulated are values of the individual nonradiative decay rates, $k_{nr,i} = k_i - k_{r,i}$, and ratios $\Phi_i = k_{r,i}/k_i$. (The Φ_i would be quantum efficiencies for the individual sublevels if SLR were so slow that they decayed independently.)

As mentioned above, for $Ir(btp)_2acac$, it was necessary to use the integrated intensities rather than the amplitudes of the decays to evaluate k_r as a function of temperature. The same procedure was tested with $Ir(ppy)_2acac$ and $Ir(piq)_2acac$. The resulting values of $k_{r,i}$, also reported in Table 3, are similar to those obtained from the amplitudes.

The steady-state spectra in Figures 7−9 were also combined with energy-level and rate parameters to extract emission spectra for the individual sublevels, $I_i(\lambda)$. It is assumed that the latter spectra are constant over the temperature range (≤50 K) used for the analysis, so that each observed $I(\lambda)$ is again a thermal average, viz.

$$I(\lambda) = \sum_i I_i(\lambda) \exp(-\beta E_i) / \sum_i \exp(-\beta E_i) \qquad (2)$$

The $I(\lambda)$ were obtained by multiplying the observed steady-state spectra by k (the effective decay rate discussed above). This procedure is rigorously correct for single-exponential decays. It appears to be valid, even with the nonexponential decays observed here, because the shape of the decay was found to be independent of λ. These spectra were obtained in arbitrary, but constant, units; the absolute intensities were not evaluated. Several low-temperature (≤50 K) spectra of $Ir(ppy)_2acac$ and $Ir(piq)_2acac$ were fit to eq 2, using the parameters listed in Table 3. For $Ir(btp)_2acac$, if $k_{r,3}$ is indeed small, it would be hard to extract a reliable spectrum for the highest sublevel. Spectra of the lower two sublevels were evaluated as the appropriate linear combinations of the spectra observed at 2 and 50 K. The resulting sublevel spectra are virtually identical to the two observed spectra in this case, whereas the spectra of the middle sublevel differs from all of the observed spectra significantly for $Ir(ppy)_2acac$ and markedly for $Ir(piq)_2acac$.

The spectra obtained for the individual sublevels are shown in the lower panels of Figures 7−9. It is interesting that the three sublevel spectra show the same trends for $Ir(ppy)_2acac$ and $Ir(piq)_2acac$. The spectrum of the highest sublevel is intermediate between the other two. Remarkably, in the case of $Ir(ppy)_2acac$, the blue edge for sublevel 3 is hypsochromically shifted, relative to that for sublevel 2 by ~93 cm^{-1}, a value that is virtually identical to the splitting between the two sublevels (90 cm^{-1}) evaluated from the excited-state lifetime data. Thus, in this one case, the difference in energy levels of the triplet sublevels can be observed in broadband spectra. For $Ir(piq)_2acac$, with a lesser splitting between the lowest and highest levels, it is hard to distinguish between a shift of the blue edge and a change in band shape.

To verify the analysis, the spectra at various other temperatures were predicted using eq 2 with the same parameters. At low temperatures, the agreement of the predicted spectra with the observed spectra is almost perfect, with just one exception noted below. To obtain good fits above approximately 140 K, it is necessary to apply a modest bathochromic shift and a broadening (convolution with a Gaussian as a function of energy) to the predicted spectra, both corrections increasing with increasing temperature. The dashed curves in Figures 7−9 are the resulting predictions at 295 K. The bathochromic shifts there are 90−150 cm^{-1} (~2−4 nm), and the rms widths of the Gaussians are 200−300 cm^{-1}, all very reasonable values. It is also necessary to multiply the predicted spectra by a factor that generally varies between 0.9 and 1.1. For $Ir(btp)_2acac$, this scaling factor may be a compensation for the neglected third sublevel; for $Ir(ppy)_2acac$ and $Ir(piq)_2acac$, it is probably just a consequence of random error in the intensities. (See Experi-

mental Section.) At 295 K, the factor was 0.92, 1.07, and 0.99 for $Ir(ppy)_2acac$, $Ir(btp)_2acac$, and $Ir(piq)_2acac$, respectively. The fact that the spectra at various temperatures over the entire range, 2−295 K, can be reproduced well by a constant set of single-sublevel spectra evaluated at low temperatures is support for the validity of the analysis and the reliability of the sublevel spectra. The one exception is that the predicted spectrum of $Ir(btp)_2acac$ at 7 K is too broad and too weak. This discrepancy vanishes if it is assumed that the actual temperature was 10 K in this one case. Making this adjustment to the temperature in the evaluation of the $k_{r,i}$ results in a slightly improved fit (not shown in Figure 10) to the rate data with the same parameters.

Relative values for the level-specific radiative rates, $k_{r,i}$, were obtained by integrating $I_i(\lambda)$ over each sublevel spectrum. The results, reported in Table 3, agree adequately with values obtained from the time-resolved measurements. From both sets of measurements, it is clear that $Ir(ppy)_2acac$ and $Ir(piq)_2acac$ have quite similar intensity patterns and that of $Ir(btp)_2acac$ is rather different.

The polarization of the emission might differ among the triplet sublevels. If the three sublevels have different polarizations, the above intensity estimates may err somewhat as a result of the polarization bias of the experiment. This issue was investigated briefly for $Ir(ppy)_2acac$ by taking low-temperature spectra with defined polarization. The excitation beam was polarized in the film plane. The emission was detected ("viewed") from a direction that was perpendicular to the electric vector of the exciting light and at 20° from the normal to the plane of the sample. That angle was small enough that outcoupling of the phosphorescence from the sample should introduce very little polarization bias. The excitation wavelength, 458 nm, was the same as for the spectra shown in Figures 7−9, and the temperatures were chosen to accentuate the contribution of each of the sublevels at least once (2, 28, 50 K). Spectra of the individual sublevels were extracted, as above, in each polarization.

The spectra of each sublevel in the two polarizations (parallel and perpendicular to that of the excitation; spectra not shown) are identical in shape and very similar to the corresponding unpolarized spectra (Figure 7, bottom panel). The emission edge for sublevel 3 is blue shifted by 160 cm^{-1} (4 nm), relative to the edge for sublevel 2, similar to the 93 cm^{-1} shift in the unpolarized spectra and the 90 cm^{-1} shift expected from the level splitting. For each sublevel, the intensity ratios of the two polarized intensities (perpendicular/parallel to the excitation) are similar, 0.8−0.9. It would be premature to make much of the polarization ratios obtained here, with excitation at a single wavelength that is significantly above the absorption edge, because the identity of the absorbing state is not rigorously established. However, the fact that the ratios are almost the same indicates that the unpolarized spectra shown in Figure 7 and analyzed for Table 3 do not introduce a significant polarization bias. Therefore, for $Ir(ppy)_2acac$, the relative intensities for the triplet sublevels that were evaluated from those unpolarized spectra can be taken at face value. Remarkably, when the two polarized spectra for each sublevel are combined with equal weights, to simulate unpolarized detection, the resulting intensity ratios (1:5.5:190) are close to those obtained from the unpolarized spectra (1:4.9:220). For $Ir(piq)_2acac$, given its similar behavior in other regards, it is reasonable to assume that its intensity data in Table 3 are also free from significant polarization bias. That assumption is more risky for $Ir(btp)_2acac$, which behaves differently in other regards. On the other hand, the differences between $Ir(btp)_2acac$ and the other complexes are so striking that, most likely, they are not a polarization artifact.

5. Discussion

As illustrated in Figures 1−6, the Shpol'skii host, *n*-octane, makes it possible to obtain high-resolution emission and excitation spectra of various nonplanar Ir(III) complexes. The line widths of a few cm^{-1} represent a great improvement over line widths in normal rigid hosts, which are usually several hundred cm^{-1} (cf. Figures 7−9). Closely related IrL_3 complexes, such as $Ir(ppy)_3$, are under development as phosphorescent dopants in organic light-emitting diodes, and the resolution afforded by the Shpol'skii host makes it possible to study model complexes, such as IrL_2acac, in much finer detail than has been possible hitherto. Survey spectra indicate that the IrL_3 complexes themselves may be amenable to study in an optimized Shpol'skii host.

Broadband spectra in an amorphous host can be obtained over a wide temperature range, they are amenable to polarization studies, and they may introduce significant new physics (e.g., disorder). Data from both narrow-line and broadband spectra have been combined to obtain radiative and nonradiative rate constants and broadband spectra for the individual triplet sublevels. In principle, all this information could be obtained from the broadband spectra alone, but the ability to analyze the broadband data consistently with the narrow-line information provides additional confidence in the methods and results. Much more information remains to be extracted, particularly from magnetic and electric field effects and polarized spectra but also from finer-grained examination of the temperature and time dependences.[27,40,53]

The relative energies of the magnetic sublevels at several sites in the Shpol'skii matrix are listed in Table 1. The lower two sublevels were observed at two prominent sites in $Ir(ppy)_2acac$ and $Ir(piq)_2acac$; and for each compound, the two sites yield similar splittings. For $Ir(btp)_2acac$, the lower two sublevels were identified for five sites, and the separation between the lower two sublevels varies considerably (19−26 cm^{-1}). In some cases, differences among the splittings are accompanied by differences in the intensity ratios, the second sublevel having somewhat larger relative intensities for sites with the smaller splittings. The varying splittings presumably reflect somewhat different molecular environments (and conformations?) of the complex in various host sites plus a sensitivity of the level-splittings to the environment. Relative oscillator strengths of the 0−0 vibronic transitions are also reported in Table 1, and lifetimes, in Table 2. The decay kinetics of the excited states suggest that the three sublevels are thermally equilibrated on the time scale of the triplet lifetime even at 2 K.

A magnetic field of 3 T has a large effect (>3×) on the intensity of the lowest sublevel in $Ir(piq)_2acac$, along with a modest 0.6 cm^{-1} shift and 1.1 cm^{-1} broadening. A similar shift, lesser broadening, and no change in intensity were observed with $Ir(ppy)_2acac$. $Ir(btp)_2acac$ was not investigated in this regard. Given the relative energy levels and intensities, a careful study of magnetic field effects might yield information on the relative polarization of the emissions and the state symmetries, even in a scattering host like polycrystalline *n*-octane.

As illustrated by Figures 7−9, the broadband spectra are remarkable. They become less intense and less "structured" at the lowest temperatures. As shown in Figure 10, both the excited-state decay rates (k, inverse lifetimes) and the radiative rates (k_r) increase dramatically with increasing temperature. The nonradiative rates (k_{nr}, not plotted) are similar (10−35% lower)

to the total decay rates (k) and also increase dramatically. The steady-state intensities represent the competition between the two strongly temperature-dependent processes. Although the steady-state intensities depend on temperature in remarkably different ways for the three complexes, the causes are actually rather subtle differences among the temperature dependences of the radiative and nonradiative decay rates in the three complexes—whether, and to what extent, the radiative rate increases more rapidly with increasing temperature than does the nonradiative rate. The changing spectral shapes can be traced back to the different spectra of the individual sublevels. The lowest sublevel has the least "structured" spectrum, and it becomes dominant only at the lowest temperatures.

Using the level separations from the Shpol'skii host as fixed parameters, the rate and spectral data were fit successfully to a simple model (eqs 1 and 2) in which the sublevels are thermally equilibrated at each temperature, and each sublevel has characteristic, temperature-independent rate constants and spectrum (i.e., k_i, $k_{r,i}$, and $I_i(\lambda)$).[27] The resulting rate constants are reported in Table 3, and the fits to the rate data are shown in Figure 10. The level-specific spectra are shown in the lower panels of Figures 7−9, and the fits at 295 K are illustrated in the upper panels (dashed curves). For $Ir(ppy)_2acac$ and $Ir(piq)_2acac$, the spectrum of the lowest sublevel differs considerably from those of the upper two sublevels, but even the latter spectra differ somewhat. For $Ir(btp)_2acac$, only the lower two sublevel spectra could be evaluated, and they again differ significantly.

The assumption of temperature-independent rate constants and spectra cannot be exactly correct, of course. As higher vibrational sublevels of the triplet state become populated at higher temperatures, the level-specific quantities probably change to some extent. The entire temperature range, up to 295 K, was used to fit the rate data, and the resulting parameters for the lower (or higher) sublevels might be more accurate representations of the low (or high) temperature values, to the extent that there is a distinction. The sublevel spectra were obtained exclusively from data at 50 K or lower and should be representative of the sublevels at low temperature. Shifts and broadenings of these sublevel spectra are presumably implied by the shifts and broadenings required to reproduce the observed spectra at higher temperatures ($\geq$140 K for $Ir(ppy)_2acac$ and $Ir(btp)_2acac$, $\geq$77 K for $Ir(piq)_2acac$; we have not investigated the onset of these changes). Even at 295 K, the observed spectra can be reproduced fairly well. The residual discrepancies might just indicate that the broadening is not purely Gaussian. The fairly good agreement of the $k_{r,i}$ values obtained from the transient measurements and from the integrated sublevel spectra tends to support the assumption that the rate parameters are constant.

It is also open to question whether only three electronic states are involved. In the case of $Ir(ppy)_2acac$, calculations indicate that there should be two triplets of different spatial symmetry separated by only ~0.01 eV, close enough that the second triplet could be populated at the higher temperatures.[34,35] The success of the present three-state model suggests that the separation is actually significantly larger. Most notably, the room-temperature spectra can be reproduced adequately using single level spectra obtained at $\leq$50 K, without invoking an additional, radiative state nearby in energy.

The fact that the energy-level data obtained from narrow-line spectra in *n*-octane can be used to fit the rate data and broadband spectra in PMMA is strong support for the present model (eqs 1 and 2). The observed lifetimes at low temperatures differ somewhat between the two hosts (Figure 10). The cause is presumably some difference in molecular environment, and it might affect the level splittings to some extent but beyond the resolution of the present data in PMMA. The nonexponential decays in PMMA might represent a disorder effect, and if so, the level splittings (and other level-specific characteristics) might actually belong to distributions with significant widths.

The oscillator-strength (f) data in *n*-octane pertain to true 0−0 bands, whereas the radiative rate constants ($k_{r,i}$) in PMMA pertain to entire emission bands. Exact agreement between the two kinds of data should not be expected, given the different band shapes (and presumably vibronic patterns) of the sublevels, and particularly not for comparisons involving the lowest sublevel (see below). Moreover, even the Shpol'skii data display a sensitivity of the properties of the sublevels to the microscopic environment, and the environment(s) in PMMA is surely different from that in *n*-octane. Nevertheless, where both kinds of data are available, they are reasonably consistent. By both measures, the lowest sublevel for each complex is the least radiative. For $Ir(piq)_2acac$, by both measures, the highest sublevel is by far the most radiative. The data on $Ir(btp)_2acac$ in PMMA were analyzed successfully with the assumption that $k_{r,3}/k_{r,2} = f_3/f_2$. The near equality of f_2/f_1 and $k_{r,2}/k_{r,1}$ obtained from this analysis, however, is probably fortuitous.

The level-specific properties of the three IrL_2acac complexes show a number of interesting regularities. For each complex, the lowest sublevel has the lowest rates of radiative and nonradiative decay. At least for $Ir(ppy)_2acac$ and $Ir(piq)_2acac$, the highest sublevel exhibits by far the highest rates. The ratio of the radiative and total decay rates (Φ_i, Table 3) varies much less—hardly at all for $Ir(ppy)_2acac$—and it varies only modestly from compound to compound. That is, the radiative and nonradiative decay rates appear to be linked, as if, perhaps, both are dominated by mixing of the triplet sublevels with just one, and the same, singlet state. The dramatically different temperature dependences of the observed steady-state intensities arise from these modest quantitative, rather than qualitative, differences among the radiative efficiencies of the three sublevels. In the sublevel spectra, the longer-wave peak or shoulder is always most prominent for the lowest sublevel, least prominent for the middle sublevel, and (for $Ir(ppy)_2acac$ and $Ir(piq)_2acac$) intermediate for the highest. The one possible exception to these regularities is the behavior of the highest sublevel of $Ir(btp)_2acac$, the complex whose observed spectra are also rather different (more "structured") from those of the other two. Because the observed rate constants vary only gradually at the higher temperatures, it is difficult to characterize that third sublevel with confidence. For instance, the ratio of radiative rates, $k_{r,3}/k_{r,2} = 0.07$, was chosen on the basis of the Shpol'skii data, but ratios as large as 0.5 can fit the data equally well.

Numerous similar complexes, including $Ir(ppy)_3$ and $Pt(ppy)_2$, share the characteristic that the lowest sublevel has both an exceptionally small oscillator strength and a vibronic pattern and/or broadband spectrum that is "anomalous".[24,25,27,31,51,52,54,55] These properties have been explained in terms of an electronically forbidden transition with Herzberg−Teller vibronic activity.[24,27] The symmetries of $Ir(ppy)_3$ and the present IrL_2acac complexes (C_3 and C_2, respectively) are low enough that all electronic transitions are formally dipole-allowed. Therefore, the weakly radiative character of the lowest sublevel cannot be explained solely in terms of the symmetries of the electronic states.

6. Summary

Narrow-line emission and excitation spectra of the lowest triplet state have been obtained in a Shpol'skii host (*n*-octane)

for three nonplanar IrL_2acac complexes of current practical interest. The spectra permit the evaluation of most of the splittings among the triplet sublevels and exhibit informative Zeeman effects. Broadband emission of the complexes in PMMA, combined with the Shpol'skii data, yield the one remaining splitting as well as properties of the individual sublevels—radiative and nonradiative decay rates and emission spectra. The data are consistent with the assumption that these individual rates and spectra are independent of temperature except for some degree of temperature-dependent broadening of the spectra. Differences between the two hosts, as well as between sites in *n*-octane, suggest a sensitivity of the parameters to molecular environment. For each complex, the decay rates of the higher sublevels are considerably larger than that of the lowest, but the radiative and nonradiative rates generally vary in parallel from one sublevel to another. The result is that the excited-state lifetime decreases rapidly with increasing temperature whereas the intensity of the emission varies more slowly. The individual sublevels have significantly different spectra. These regularities appear to be universal characteristics of Ir(III) and Pt(II) complexes. They cannot be explained on the basis of symmetry alone, because the present complexes, as well as $Ir(ppy)_3$, have such low symmetry that all transitions are electronically dipole-allowed once spin−orbit interaction breaks the spin-selection rule. At least in such low-symmetry cases, these regularities remain unexplained, and an explanation is likely to shed new light on the factors governing radiative and nonradiative decay rates in these complexes—the quantities that make them attractive as phosphorescent dopants. The present study was undertaken as a preliminary survey, and much more information remains to be extracted from the spectra, and particularly the Shpol'skii spectra, of these intriguing compounds.

Acknowledgment. We thank J. M. Hodes for invaluable technical assistance, D. Y. Kondakov and M. E. Wojcik-Cross for the solution data, M. Rajeswaran for the X-ray structure determination, and D. J. Giesen for numerous informative discussions and computations.

References and Notes

(1) Baldo, M. A.; O'Brien, D. F.; You, Y.; Shoustikov, A.; Sibley, S.; Thompson M. E.; Forrest, S. R. *Nature* **1998**, *395*, 151.

(2) O'Brien, D. F.; Baldo, M. A.; Thompson, M. E.; Forrest, S. R. *Appl. Phys. Lett.* **1999**, *74*, 442.

(3) Baldo, M. A.; Lamansky, S.; Thompson, M. E.; Forrest, S. R. *Appl. Phys. Lett.* **1999**, *75*, 4.

(4) Adachi, C.; Baldo, M. A.; Forrest, S. R.; Thompson, M. E. *Appl. Phys. Lett.* **2000**, *77*, 904.

(5) Adachi, C.; Baldo, M. A.; Thompson, M. E.; Forrest, S. R. *J. Appl. Phys.* **2001**, *90*, 5048.

(6) King, K. A.; Spellane, P. J.; Watts, R. J. *J. Am. Chem. Soc.* **1985**, *107*, 1431.

(7) Sandrini, D.; Maestri, M.; Ciano, M.; Balzani, V.; Lueoend, R.; Deuschel-Cornioley, C.; Chassot, L.; von Zelewsky, A. *Gaz. Chim. Ital.* **1988**, *118*, 661.

(8) Dedeian, K.; Djurovich, P. I.; Garces, F. O.; Carlson, G.; Watts, R. J. *Inorg. Chem.* **1991**, *30*, 1687.

(9) Lamansky, S.; Djurovich, P.; Murphy, D.; Abdel-Razzaq, F.; Kwong, R.; Tsyba, I.; Bortz, M.; Mui, B.; Bau, R.; Thompson, M. E. *Inorg. Chem.* **2001**, *40*, 1704.

(10) Lamansky, S.: Djurovich, P.; Murphy, D.; Abdel-Razzaq, F.; Lee, H.-E.; Adachi, C.; Burrows, P. E.; Forrest, S. R.; Thompson, M. E. *J. Am. Chem. Soc.* **2001**, *123*, 4304.

(11) Kawamura, Y.; Goushi, K.; Brooks, J.; Brown, J. J.; Sasabe, H.; Adachi, C. *Appl. Phys. Lett.* **2005**, *86*, 071104.

(12) Ikai, M.; Tokito, S.; Sakamoto, Y.; Suzuki, T.; Taga, Y. *Appl. Phys. Lett.* **2001**, *79*, 156 and references cited.

(13) Markham, J. P. J.; Lo, S.-C.; Magennis, S. W.; Burn, P. L.; Samuel, I. D. W. *Appl. Phys. Lett.* **2002**, *80*, 2645.

(14) Li, J.; Djurovich, P. I.; Alleyne, B. D.; Yousufuddin, M.; Ho, N. N.; Thomas, J. C.; Peters, J. C.; Bau, R.; Thompson, M. E. *Inorg. Chem.* **2005**, *44*, 1713.

(15) Sprouse, S.; King, K. A.; Spellane, P. J.; Watts, R. J. *J. Am. Chem. Soc.* **1984**, *106*, 6647.

(16) Ichimura, K.; Kobayashi, T.; King, K. A.; Watts, R. J. *J. Phys. Chem.* **1987**, *91*, 6104.

(17) Brooks, J.; Babayan, Y.; Lamansky, S.; Djurovich, P. I.; Tsyba, I.; Bau, R.; Thompson, M. E. *Inorg. Chem.* **2002**, *41*, 3055.

(18) Tamayo, A. B.; Alleyne, B. L.; Djurovich, P. I.; Lamansky, S.; Tsyba, I.; Ho, N. N.; Bau, R.; Thompson, M. E. *J. Am. Chem. Soc.* **2003**, *125*, 7377.

(19) Tsuboyama, A.; Iwawaki, H.; Furugori, M.; Mukaide, T.; Kamatani, J.; Igawa, S.; Moriyama, T.; Miura, S.; Takiguchi, T.; Okada, S.; Hoshino, M.; Ueno, K. *J. Am. Chem. Soc.* **2003**, *125*, 12971.

(20) Goushi, K.; Kawamura, Y.; Sasabe, H.; Adachi, C. *Jpn. J. Appl. Phys.* **2004**, *7A*, L937.

(21) Kawamura, Y.; Gouchi, K.; Brooks, J.; Brown, J. J.; Sasabe, H.; Adachi, C. *Appl. Phys. Lett.* **2005**, *86*, 071104.

(22) Nam, E. J.; Kim, J. H.; Kim, B.-O.; Kim, S. M.; Park, N. G.; Kim, Y. S.; Kim, Y. K.; Ha, Y. *Bull. Chem. Soc. Jpn.* **2004**, *77*, 751.

(23) Dedian, K.; Shi, J.; Shepherd, N.; Forsythe, E.; Morton, D. C. *Inorg. Chem.* **2005**, *44*, 4445.

(24) Yersin, H.; Donges, D. *Top. Curr. Chem.* **2001**, *214*, 81 and references cited.

(25) Colombo, M. C.; Hauser, A.; Güdel, H. U. *Inorg. Chem.* **1993**, *32*, 3088.

(26) Colombo, M. C.; Brunold, T. C.; Riedener, T.; Güdel, H. U.; Förtsch, M.; Bürgi, H.-B. *Inorg. Chem.* **1994**, *33*, 545.

(27) Finkenzeller, W. J.; Yersin, H. *Chem. Phys. Lett.* **2003**, *377*, 299.

(28) Finkenzeller, W. J.; Stössel, P.; Yersin, H. *Chem. Phys. Lett.* **2004**, *397*, 289.

(29) Yersin, H.; Donges, D.; Humbs, W.; Strasser, J.; Sitters, R.; Glasbeek, M. *Inorg. Chem.* **2002**, *41*, 4915.

(30) Goushi, K.; Kwong, R.; Brown, J. J.; Sasabe, H.; Adachi, C. *J. Appl. Phys.* **2004**, *95*, 7798.

(31) Strasser, J.; Homeier, H. H. H.; Yersin, H. *Chem. Phys.* **2000**, *255*, 301.

(32) Wilde, A. P.; King, K. A.; Watts, R. J. *J. Phys. Chem.* **1991**, *95*, 629.

(33) Stückl, A. C. *Coord. Chem. Rev.* **1997**, *159*, 407.

(34) Giesen, D. J. Personal communication.

(35) Hay, P. J. *J. Phys. Chem. A* **2002**, *106*, 1634.

(36) Pierloot, K.; Ceulemans, A.; Merchán, M.; Serrano-Andrés, L. *J. Phys. Chem.* **2000**, *104*, 4374.

(37) McClure, S. *Electronic Spectra of Molecules and Ions in Crystals*; Academic Press: New York, 1959; Part 1.

(38) Marchetti, A. P.; Landry, J. F.; Tinti, D. S. *J. Chem. Phys.* **1974**, *61*, 1086.

(39) Marchetti A. P.; M. Scozzafava, M. *J. Chem. Phys.* **1976**, *65*, 2382.

(40) Güntner, W.; Gliemann, G. *J. Phys. Chem.* **1990**, *94*, 618.

(41) Shpol'skii, E. V. *Sov. Phys. Usp.* **1960**, *3*, 372 (English Translation).

(42) Garrigues, P.; Budzinski, H. *Trends Anal. Chem.* **1995**, *14*, 231.

(43) Eberly, J. H.; McColgin, W. C.; Kawaoka, K.; Marchetti, A. P. *Nature* **1974**, ***251***, 215.

(44) McColgin, W. C.; Marchetti, A. P.; Eberly, J. H. *J. Am. Chem. Soc.* **1978**, *100*, 5622.

(45) Su, Y.-J.; Huang, H.-L.; Li, C.-L.; Chien, C.-H.; Tao, Y.-T.; Chou, P.-T.; Datta, S.; Liu, R.-S. *Adv. Mater.* **2005**, *15*, 884.

(46) Kamatani, J.; Okada, S.; Tsuboyama, A.; Takiguchi, T.; Miura, S.; Noguchi, K.; Moriyama, T.; Igawa, S.; Furugori, M. U.S. Patent Application 0068526 A1, 2003.

(47) Marchetti, A. P.; Rodney, P. J.; von der Osten, W. *Phys. Rev. B* **2001**, *64*, 132201.

(48) Carrington, A.; McLachlan, A. D. *Introduction to Magnetic Resonance*; Harper and Row: New York, 1967; Chapter 8.

(49) Poole C. P.; Farach, H. A. *Theory of Magnetic Resonance*; John Wiley and Sons: New York, 1987; Chapter 8.

(50) McCauley, E. M.; Lasko C. L.; Tinti, D. S. *J. Phys. Chem.* **1992**, *96*, 1146.

(51) Striplin, D. R.; Crosby, G. A. *Chem. Phys. Lett.* **1994**, *221*, 426.

(52) Harrigan, R. W.; Crosby, G. A. *J. Chem. Phys.* **1973**, *59*, 3468.

(53) Stampor, W.; Mezyk, J.; Kalinowski, J. *Chem. Phys.* **2004**, *300*, 189.

(54) Watts, R. J.; Harrigan, R. W.; Crosby, G. A. *Chem. Phys. Lett.* **1971**, *8*, 49.

(55) Yersin, H.; Humbs, W.; Strasser, J. *Top. Curr. Chem.* **1997**, *191*, 153.